Green Chemistry

PAPER

View Article Online
View Journal | View Issue

Cite this: *Green Chem.*, 2025, **27**, 1073

Sustainable regeneration of cathode active materials from spent lithium-ion batteries by repurposing waste coffee powder†

Md. Anik Hasan,[a,b] Rumana Hossain *[a] and Veena Sahajwalla[a]

To develop sustainable recycling methods for spent lithium-ion batteries (LIBs), the use of renewable materials and minimizing energy consumption are essential. Here, we propose a biomass-based, energy-intensive reduction method to recover Li and Co from spent LIBs. Waste coffee powder was used as a biomass to provide carbon and reducing gas during the reduction process. During selective thermal transformation, the carbon and reducing gas derived from waste coffee powder converted the cathode material of LIBs $LiCoO_2$ into Li_2CO_3 and Co/CoO, recovering 89.23% of Li and 93.27% of Co. Compared to the conventional carbothermic reduction process, this transformation occurred at a lower temperature (600 °C) due to the synergetic effect of reducing gas and carbon. Moreover, $LiCoO_2$ was regenerated from the recovered Li_2CO_3 and Co/CoO, demonstrating excellent electrochemical performances in terms of charge–discharge capacity, cyclic performance, rate performance, EIS, and CV curve analysis. An EverBatt-based environmental and economic analysis shows that this reduction method reduces greenhouse gas (GHS) emissions and energy consumption, making it economically viable. Overall, this research offers an eco-friendly and energy-efficient method to recycle spent LIBs using waste biomass. Additionally, this study will contribute to achieving several Sustainable Development Goals (SDGs).

Received 9th October 2024,
Accepted 20th November 2024

DOI: 10.1039/d4gc05048g

rsc.li/greenchem

1. Introduction

Due to their environmental friendliness, high working voltage, rechargeability, high power density and longer lifespan, the use of lithium-ion batteries (LIBs) is increasing daily worldwide. LIBs are playing a vital role in supporting a fuel-free economy, and it is estimated that they contribute about 37% of the global battery market.[1] Lithium possesses several advantageous properties, such as a higher heat capacity (3.489 J g^{-1} mol^{-1}) and higher redox potential (93.045 V) than other metals such as zinc. These properties are expected to drive LIBs' increasing contribution to the battery market in the near future.[2] LIBs are used in cellular phones, portable devices, electric vehicles, laptops, medical equipment, and sophisticated electronic devices. Due to their versatile applications, the demand for LIBs has been rising steadily.[3] In recent years the production and utilization of electric vehicles have increased significantly which could reduce CO_2 emission. Zhang and Zhu[4] reported that maximum portion of global CO_2 emission is generated from the transportation industry especially from cars. For this reason, a massive conversation is happening globally regarding the energy storage system of the vehicle industry. In 2021, with a growth rate of more than 100% around 6.75 million electric vehicles were vented throughout the world.[5] Most of these electric vehicles utilize LIBs as their power source because of their long life and high energy and power density. The rapid use of LIBs resulted in the generation of a significant number of spent LIBs. Depending on the utilization style, the average operating life of a LIB is approximately 3 to 8 years.[6] However, it is estimated that the global recycling market of LIBs will reach $23.72 billion by 2030.[7] Improper management of spent LIBs, along with the toxic electrolytes and heavy metals they contain, can have a detrimental impact on the environment and human health.[8] Additionally, to meet the global demand for critical minerals, the LIB industry must focus on recycling spent LIBs and recovering valuable metals.[9] The scarcity and high utilization of lithium have also promoted increased attention on the recovery process of spent LIBs.[10]

Traditionally, three methods are commonly used for the recovery of waste LIBs, that is hydrometallurgy, pyrometallurgy, and biometallurgy.[11] Among these, the hydrometallurgical

[a]*Centre for Sustainable Materials Research & Technology, SMaRT@UNSW, School of Materials Science and Engineering, UNSW Sydney, Australia.*
E-mail: r.hossain@unsw.edu.au
[b]*Department of Leather Engineering, Khulna University of Engineering and Technology (KUET), Khulna, 9203, Bangladesh*

† Electronic supplementary information (ESI) available. See DOI: https://doi.org/10.1039/d4gc05048g

method is the most widely used and considered the most promising recycling process due to its low impurity content, high leaching efficiency, and selective metal recovery capabilities.[12] The hydrometallurgical process involves dissolving spent cathode materials in organic or inorganic acids, followed by separation techniques like ion exchange, chemical precipitation, and solvent extraction.[13] However, the involvement of multiple steps and extensive use of reductant and concentrated acid results in a high volume of effluent, leading to secondary pollution through the release of gas and acidic wastewater during the leaching process.[14] From both environmental and economic viewpoints, the biometallurgy method has been considered the most promising recycling process. However, its slow operation time and process efficiency have hindered its development.[15] To achieve the performance from the bacteria used in the biometallurgy leaching processes, factors such as temperature, pH, salt content and moisture content must be carefully controlled, making the process more complex.[16] Currently, the pyrometallurgy process is considered the most mature recovery technology and is widely used in various industries due to its short operation time, reduced production of liquid waste, and lower raw material requirements.[17] Nevertheless, the pyrometallurgy method has some drawbacks, such as high temperature risk, high energy consumption, the tendency to produce toxic gas, and high operational cost.[18] Recently, the pyrometallurgy method running at medium temperatures has gained popularity due to its environmental friendliness and low energy consumption.[19]

The current medium-temperature pyrometallurgy method is primarily a carbothermic reduction process, regulated by carbon-based materials. Park *et al.*[20] conducted a carbothermic reduction process at temperatures between 600 and 800 °C in the presence of CO_2 to recover Li in the form of Li_2CO_3 from spent LIBs. Nuraeni *et al.*[21] used graphite as a reductant in the carbothermic reduction of spent LIBs' cathode materials and recovered Co, Li_2O, and Li_2CO_3 under an argon gas atmosphere at temperatures between 700 and 1100 °C. Yan *et al.*[22] applied a combination of carbothermic reduction followed by a water leaching process for the recovery of Li from spent cathode materials and recovered more than 93% of Li as $LiCO_3$ and LiOH from 800 to 900 °C. In another study, Zhang *et al.*[23] utilized a mixture of spent cathode materials and lignite to extract 85% of Li through carbonization. The use of H_2 as a reducing agent has advantages over carbothermal reduction as it reduces both the operational time and temperature. Thus, the carbothermal reduction process typically employs hydrogen, carbon, and their associated compounds.[24] Photosynthesis-derived waste biomass also contains hydrogen and carbon, making it a viable source for the carbothermal reduction process.[25] Zhao *et al.*[26] used biomass pyrolysis and microwave heating to reduce spent LIBs to Li_2CO_3 and recover 93% of Li. Recently, waste biomass-based materials have attracted much more attraction as a feedstock for the reduction of spent LIBs. Zhou *et al.*[27] have used waste pine sawdust as a biomass source for the reduction of spent LIBs and recovered 94% of Li and 97% of Co. In another study, Zhou *et al.*[28] investigated the suitability of the pyrolysis gas generated from different biomass such as waste wood, corn, rice husk and kraft paper for the reduction of $LiCoO_2$. Among waste biomass materials, spent coffee powder is considered one of the most promising reducing agents and has been applied in various fields, including steelmaking,[29] SiC nanomaterials production,[30] and reduction of pollutants from wastewater.[31] Coffee is the second most consumed beverage globally, with an annual production of around sixty million tons.[33] Approximately half of this coffee is turned into waste coffee grounds, and this significant volume of waste is typically disposed of in landfills, where it releases greenhouse gases such as carbon dioxide and methane.[32,33] As a result, finding sustainable ways to utilize this solid waste has become a growing concern. Lee *et al.*[34] reported that waste coffee powder has a higher effective hydrogen-to-carbon ratio (H/Ceff) than wood-based biomass, making it a suitable feedstock for thermochemical conversion.

In the present study, waste biomass was utilized as a reducing agent to develop carbon-neutral technology to recover metals from $LiCoO_2$-containing spent LIBs through the pyrometallurgical process. For the first time waste coffee powder was selected as the biomass source for reducing the spent $LiCoO_2$, in which waste coffee powder is acting as a reducing agent during the thermal transformation process. The waste coffee powder-assisted carbothermic reduction process was conducted under controlled experimental conditions at temperatures ranging from 400 °C to 800 °C. Following the reduction, the water leaching process was applied to separate and recover Li_2CO_3 and CoO, or Co. $LiCoO_2$ was regenerated from the recovered Li_2CO_3 and CoO/Co through the pyrometallurgy process. Regenerated $LiCoO_2$ was characterized through X-ray diffraction (XRD), Raman analysis, scanning electron microscopy (SEM), Brunauer–Emmett–Teller (BET) analysis, and X-ray photoelectron spectroscopy (XPS). Finally, the regenerated $LiCoO_2$ was employed as a cathode material and its electrochemical performance was evaluated by analyzing different parameters such as charge–discharge capacity, cyclic performance, rate performance, EIS, and CV curves.

2. Materials and methods

2.1 Materials

Waste coffee powder was collected from a local coffee shop in Sydney, Australia. Spent LIBs were collected from a battery recycling center. To discharge the spent LIBs, they were immersed in a 5 wt% NaCl solution for 12 hours. Afterward, the batteries were vacuum-dried for 12 hours at 100 °C. The anode and cathode materials were then manually disassembled in a glovebox. To remove the organic matter, the cathode materials were placed in a tube furnace and pyrolyzed for 1 hour at 450 °C. Following this, the positive electrode powder and the current collector were manually peeled off. The battery chemistry of LIBs is often between manufacturers, but in this study, only those containing $LiCoO_2$ as the active

Table 1 Amount of elements present in the cathode powder

Element Unit	Li % wt	Co % wt	Ni mg kg^{-1}	Cr mg kg^{-1}	Al mg kg^{-1}	Cu mg kg^{-1}	Mn mg kg^{-1}	Ti mg kg^{-1}	P mg kg^{-1}
Cathode powder	7.23	55.02	123.46	4.89	621.38	4.46	18.23	13.01	133.31

cathode material were used. The elemental composition of the cathode material is shown in Table 1.

2.2 Cathode material recycling and reduction

Three reduction methods, *i.e.* biochar reduction, gas reduction, and coffee powder reduction, were analyzed by three mixing methods. The schematic diagram of the three-reduction process is shown in Fig. 1.

For coffee powder reduction, a different portion of waste coffee powder was mixed homogeneously with different portions of $LiCoO_2$ in an agate mortar. The mixture was then placed in a tube furnace and heat-treated for 90 min in the temperature range of 400–800 °C. A portion of the heat-treated powder was dissolved in aqua regia ($HCl:HNO_3$ = 3 : 1 in volume ratio) solution to measure the concentration of Li and Co. The remainder of the heat-treated powder was subjected to water leaching. During the water leaching process, the powder was placed in deionized water, maintaining a solid-to-liquid ratio of 20 g L^{-1}, and soaked for 30 min at room temperature. The water leachate was then filtered through a Whatman filter paper. Solid particles were deposited on the filter paper while the filtrate was dried in a blast drying box to obtain the precipitate.

For biochar reduction, waste coffee powder was carbonized in a tube furnace for 120 minutes at a constant temperature of 500 °C. Afterward, the carbonized coffee powder was mixed homogeneously with $LiCoO_2$ in an agate mortar. The mixture was then transferred to the tube furnace and heated for 90 minutes within the temperature range of 400–800 °C. After thermal transformation, the products were treated the same as the coffee powder reduction. In the case of gas reduction, $LiCoO_2$ and waste coffee powder were placed in a cuvette separately which was covered with a clip boat. The cuvette was then placed in a tube furnace and heat treated for 90 min in the temperature range from 400–800 °C. After heat treatment, the treatment for the powder followed the same process as for both coffee powder reduction and biochar reduction. The experimental set-up diagram for the three-reduction approach is shown in Fig. S1, S2, and S3.†

2.3 Regeneration process

At 750 °C temperature, the recovered CoO was calcined for 30 min to convert it to Co_3O_4. Then through the solid phase reaction of Li_2CO_3 and Co_3O_4, $LiCoO_2$ was regenerated. In this method, the calcination process was carried out for 13 hours at 950 °C temperature. To compensate for Li_2CO_3 evaporation at a high-temperature process, the Li/Co ratio was set at 1.15.

2.4 Characterization

The degradation mechanism and thermal transformation of the waste coffee powder and the mixture of waste coffee powder and $LiCoO_2$ were determined by utilizing a thermal analyzer (STA 8000, PerkinElmer), under a N_2 gas atmosphere. The phase composition and crystal structures of the thermally treated powder materials were determined using a PANalytical Empyrean II X-ray diffraction (XRD) system using Co Kα radiation (λ = 1.789 Å) in the range of 15° ≤ 2θ ≤ 90°. The obtained data were analyzed by utilizing HighScore Plus software. The concentration of metals in the leachate was analyzed through an atomic absorption spectrophotometer (AAS, TAS-990). The

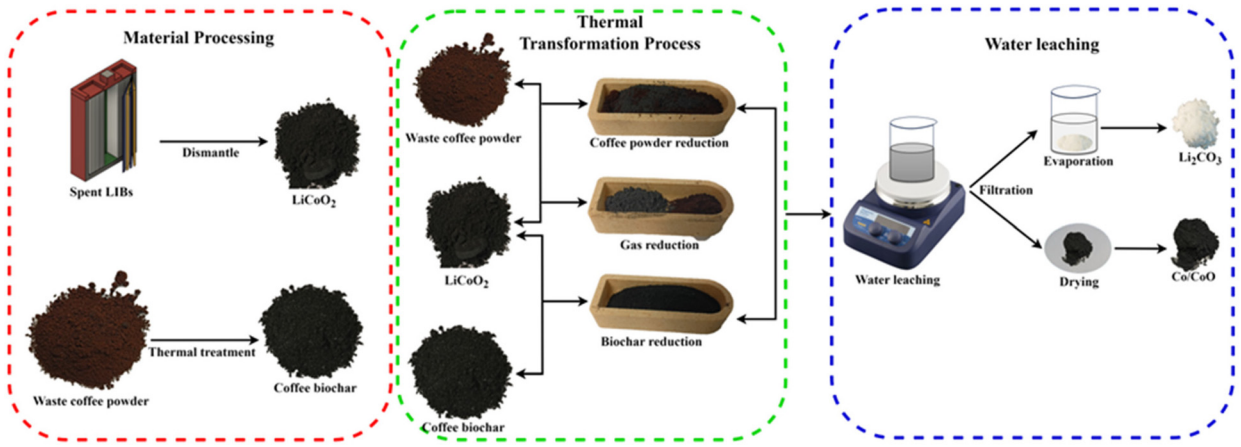

Fig. 1 Schematic diagram of the whole methodology.

recovery efficiency of Li and Co from the spent LIBs was calculated by using the following equation:

$$R(\%) = \frac{A_i}{A_m} \times 100 \quad (1)$$

where A_i is the number of moles of recovered elements; A_m is the number of moles of elements present in the mixed powder.

To observe the microstructure and surface morphology of the samples, a field emission scanning electron microscope (FE-SEM) (Nova NanoSEM 450) was used. The pore diameter, particle size, and surface area of the samples were measured by Brunauer–Emmett–Teller (BET) analysis and the Barrett–Joyner–Halenda (BJH) method. The binding energy and distribution density of the elements present in the samples were determined by using X-ray photoelectron spectroscopy (ESCALAB 250Xi, Thermo Scientific, UK). For the XPS analyzer, the X-ray source was monochromatic Al Kα ($h\upsilon$ = 1486.68 eV) rays. With a take-off angle of 90° and an ultrahigh vacuum (~2 × 10^{-9} mbar), XPS analysis was carried out where graphite was used as the binding energy reference.

2.5 Electrochemical measurement

To analyze the electrochemical performance of the regenerated $LiCoO_2$, a CR2016 coin cell was prepared. For making the electrodes, regenerated $LiCoO_2$, acetylene black, and polyvinylidene fluoride were mixed homogeneously at a mass ratio of 8 : 1 : 1. To make a slurry *N*-methyl-2-pyrrolidone was added to the powder mixture and the slurry was stirred for 24 h at 600 rpm to make the slurry more homogeneous. Then the slurry was coated at a thickness of 0.1 mm onto an aluminum foil and dried at 80 °C for 12 h in a vacuum oven. To enhance the adhesion between the aluminum foil and pasted coat, after drying the coated sheet was pressed for 1 h at 100 kN pressure by utilizing a flat-plate presser. Then the electrode was cut into a disk-like shape with an average diameter of 12 mm and the average weight of the regenerated $LiCoO_2$ in each disc was around 3.5–3.8 mg. The disc-like electrode was then transferred to an argon-filled glovebox and assembled there. Where 1 M $LiPF_6$ was used as an electrolyte, metallic lithium was employed as a counter electrolyte and 14 mm glass fiber was utilized as a separator. By utilizing Neware battery testers, the galvanostatic charge/discharge capacity of the produced battery was analysed.

2.6 Environmental and economical impact analysis

To carry out the life-cycle and techno-economical analysis of hydrometallurgical, pyrometallurgical, and current biomass reduction processes, the EverBatt closed-loop battery recycling model is used.[35] In our study, we consider GHG emissions and total energy use in the three-recycling process while emission and energy use in the transportation were not included. Besides, the revenue and cost associated with the three-recycling methods were also calculated by following the above-mentioned model.

Generally, the hydrometallurgy recovery process consists of three steps: dismantling, heating, and leaching. In the first step, the waste LIBs are discharged and crushed, and then the electrolytes and binders are burned at a lower temperature. To isolate plastic, steel, copper, and aluminum, different physical processes are applied. Finally, to recover Li and Co compounds, several leaching processes are used. The hydrometallurgy recovery process used in the EverBatt model is illustrated in Fig. S4.†

In the common pyrometallurgy recovery process, initially, the waste LIBs are mechanically pretreated such as crushing, sieving, and milling. Then, the organic solvent and electrolyte were heat treated at 150–500 °C temperature. Finally, by adding a reducing agent (activated carbon, graphite, aluminum foil, NH_4Cl, $CaCl_2$, $NaHSO_4$) and slag modifiers (SiO_2, CaO, Al_2O_3, MgO), the materials are treated at high temperatures (1400–1700 °C). The pyrometallurgy process developed in the EverBatt model is shown in Fig. S5.†

In our study, to explain the biomass reduction recovery process, the direct recovery process present in EverBatt's model is modified. The recovery steps followed in this research are presented in Fig. S6.† In this recovery process, four steps are mainly involved namely dismantling, heating at a lower temperature, biomass reduction, and water leaching. After dismantling the heating process is applied to isolate the electrode materials and burn the binder. In the second heat treatment, the cathode material ($LiCoO_2$) is burned with biomass (waste coffee powder) without adding other chemicals. Another important thing is that in the whole recovery process, no strong solvents, alkalis, or acids are used.

2.7 Assessment of greenhouse gas emissions and energy consumption

2.7.1 Material input. The input materials that are used in the three recycling methods are presented in Table 2. The material required for the hydrometallurgical and pyrometallurgical recovery process is collected from the EverBatt model. On the other hand, the materials required for the present study are picked up according to our recovery process.

2.7.2 Energy input. The energy consumed in the recovery process is calculated through life cycle analysis. The LCA includes the environmental impact of power generation, fuel production, and on-site fuel combustion (natural gas/diesel combustion). In LCA we also examined the environmental impact which is related to process emissions.

Table 2 Required materials for the recycling of 1 kg waste LIB through different recycling methods

Hydrometallurgy	Pyrometallurgy	Direct recycling
Sulfuric acid	Sand	Waste coffee powder
Hydrochloric acid	Limestone	
Ammonium hydroxide	Hydrogen peroxide	
Sodium hydroxide	Hydrochloric acid	
Soda ash		
Hydrogen peroxide		

3. Results and discussion

3.1 Thermogravimetric analysis

The thermogravimetric analysis of the waste coffee powder and the mixture of waste coffee powder and $LiCoO_2$ is illustrated in Fig. 2. From Fig. 4a it is observed that in the temperature zone of 42–232 °C coffee powder loses a small amount of weight (3.76%) and the reason behind this is the loss of water when the heating process is carried out. The maximum mass loss of the coffee powder (94.55%) occurred between the temperature of 232 °C and 424 °C. An exothermic peak is also observed in this temperature zone and because of the conversion of coffee powder into biochar, gas, and bio-oil, this huge amount of mass loss occurred.

Until temperature 400 °C the weight loss pattern of the mixture of coffee powder and $LiCoO_2$ is almost similar to the pure coffee powder. The mixed sample mass loss mainly takes place in three temperature zones of 200–400 °C, 400–700 °C and 700–850 °C, and the maximum mass loss was observed in the temperature range of 200–400 °C. The exothermic peak at 311 °C stipulates that at this temperature the coffee powder reduction reaction has occurred. In the temperature range of 400–700 °C, there are two absorption peaks which indicate that a reduction reaction between the $LiCoO_2$ and gas takes place in this temperature zone. Another peak at temperature 685 °C is observed which might be due to the reduction of CoO. Between the temperature 700–850 °C the mass loss of the mix sample is 10.85% and there are two absorption peaks, suggesting that carbothermal reduction of $LiCoO_2$ occurred by biochar in this temperature zone. After a temperature of 700 °C the rate of weight loss is faster indicating the generation of Li_2CO_3 and CO_2 from Li_2O and coffee powder respectively.

By following a thermodynamic study, the phase changes of $LiCoO_2$ during the reduction reaction can be analyzed. $LiCoO_2$ is decomposed as follows:

$$4LiCoO_2 = 4CoO + 2Li_2O + O_2(g). \quad (2)$$

When the coffee powder goes through the thermal transformation process not only biochar but also H_2, CO_2, and CO gases will be produced (Fig. S7†). The generated gaseous substances reduced $LiCoO_2$ to CoO and above 700° C $LiCoO_2$ is reduced by the C under a N_2 atmosphere.

$$8LiCoO_2 + 4H_2\ (g) = 8CoO + 4Li_2O + 4H_2O \quad (3)$$

$$8LiCoO_2 + 2CO_2\ (g) = 4Li_2CO_3 + 8CoO \quad (4)$$

$$2LiCoO_2 + CO\ (g) = 2CoO + Li_2O + CO_2\ (g) \quad (5)$$

$$4LiCoO_2 + C = 4CoO + 2Li_2O + CO_2\ (g) \quad (6)$$

Again, CoO is reduced by the generated H_2, CO, and biochar to Co.

$$4CoO + 2H_2\ (g) = 4Co + 2H_2O\ (g) \quad (7)$$

$$CoO + CO\ (g) = Co + CO_2\ (g) \quad (8)$$

$$2CoO + C = 2Co + CO_2\ (g) \quad (9)$$

Next, the produced CO_2 and C can combine and form CO. When the reduction process takes place CO_2 could combine with Li_2O and produce Li_2CO_3.

$$CO_2\ (g) + C = 2CO \quad (10)$$

$$CO_2\ (g) + Li_2O = Li_2CO_3 \quad (11)$$

Fig. 3 manifests the relationship of the change of the standard Gibbs free energy ΔG^{θ} with the temperature for reactions (3)–(11). According to thermodynamics, for a particular reaction if the value of the Gibbs free energy ΔG^{θ} is negative then we can say that this reaction has occurred spontaneously. In reactions (3) and (6), $LiCoO_2$ is reduced by H_2 and C and the value of ΔG^{θ} is positive until the temperature of 420 °C and 257 °C respectively. Whereas for reactions (4) and (5) where $LiCoO_2$ is reduced by CO_2 and CO, the value of ΔG^{θ} is negative for the entire temperature range. This means $LiCoO_2$ is more easily reduced by CO_2 and CO than H_2 and C. In reaction (8), CO reduced CoO and the

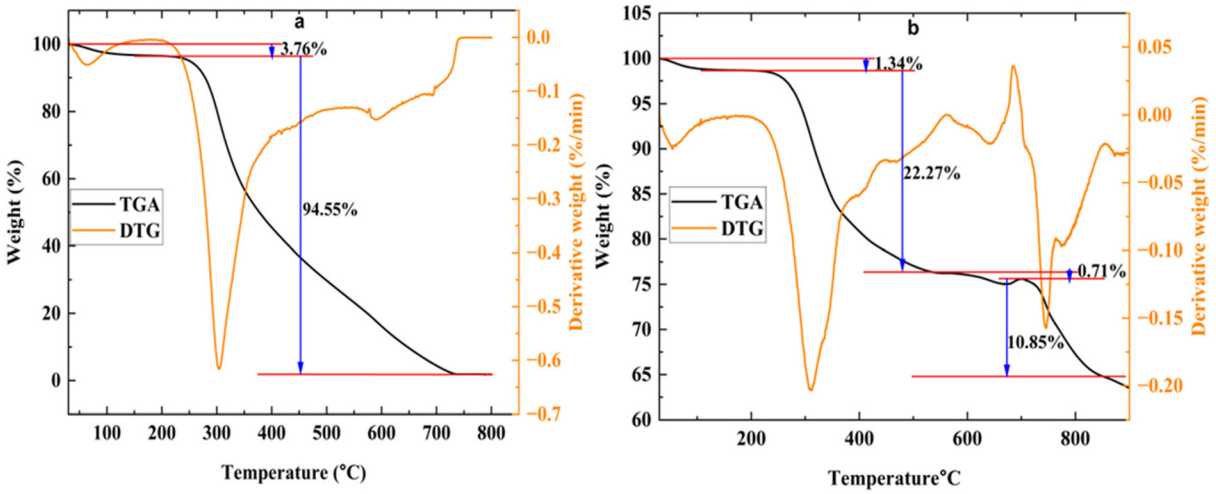

Fig. 2 TGA-DTG curves of (a) waste coffee powder and (b) a mixture of waste coffee powder and $LiCoO_2$ (mass ratio 1 : 1).

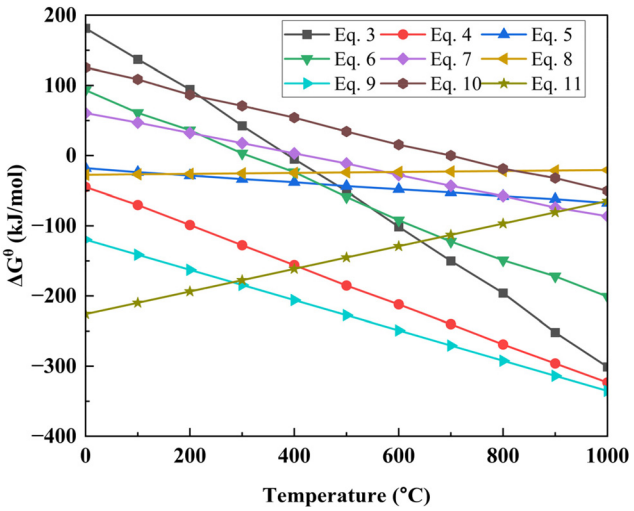

Fig. 3 Relationship between the Gibbs free energy (ΔG^{θ}) and the temperature of the chemical reactions occurring during the reduction process.

reaction occurred spontaneously in the whole temperature range, while in reactions (7) and (9) where CoO is reduced by H_2 and C, the value of ΔG^{θ} is positive below the temperature 480 °C and 316 °C respectively. These results show almost similar phenomena when the reduction of $LiCoO_2$ occurs. Below the temperature 573 °C, the value of ΔG^{θ} remains positive for reaction (10) which indicates the presence of CO_2 in the gas reduction process. In reaction (11), the produced product is Li_2CO_3 and the value of ΔG^{θ} for this reaction is negative for the whole temperature range which indicates that even in the low temperature reduction process Li_2CO_3 exists in the system.

3.2 Waste coffee powder reduction thermal transformation

Fig. 4a illustrates the XRD pattern of the waste coffee powder reduction thermal transformation which was performed at a ratio of 1 : 1 (CP : $LiCoO_2$) for 90 min at temperatures of 400 °C, 500 °C, 600 °C, 700 °C, and 800 °C. From the figure it has been observed that at 400 °C no $LiCoO_2$ is present in the obtained products, the potential reason for this phenomenon is that due to the effect of biochar and gas, $LiCoO_2$ is converted into more stable Li_2CO_3 and CoO. On further increasing the temperature, the reduction rate is also gradually increased, which is why CoO is converted to Co and the amount of Li_2CO_3 is decreased. At a temperature of 800 °C, the products only contain Li_2O and Co. The absence of Li_2CO_3 at higher temperatures is observed because of the decomposition and vaporization characteristics of Li_2CO_3 at higher temperatures which creates difficulties for XRD to detect it. Depending on the carbon content, different products can be obtained by modifying the temperature.

Fig. 4b presents the XRD pattern of the coffee powder reduction products in different mass ratios of coffee powder and $LiCoO_2$ at 600 °C temperature for 90 min. From the figure, it is observed that with the decreasing mass ratio of coffee powder and $LiCoO_2$, in the main product, the Co content also gradually decreases. Decreasing the coffee powder content reduces the availability of C and H_2 in the reaction, resulting in only CoO being present in the final product when the mass ratio of coffee powder to $LiCoO_2$ is 1 : 5. So, by changing the mass ratio of coffee powder and $LiCoO_2$ the thermodynamic behavior can be changed to obtain different products.

3.3 Syngas and biochar reduction thermal treatment

The XRD pattern of the product obtained from the gas and biochar reduction thermal transformation for 90 min at different temperatures is presented in Fig. 5(a and b). From the gas reduction diffraction peaks, it has been observed that $LiCoO_2$ is present in the products after reduction at 400 °C and 500 °C which is dissimilar to the coffee powder reduction (Fig. 5a). The possible reason for this dissimilarity is that the

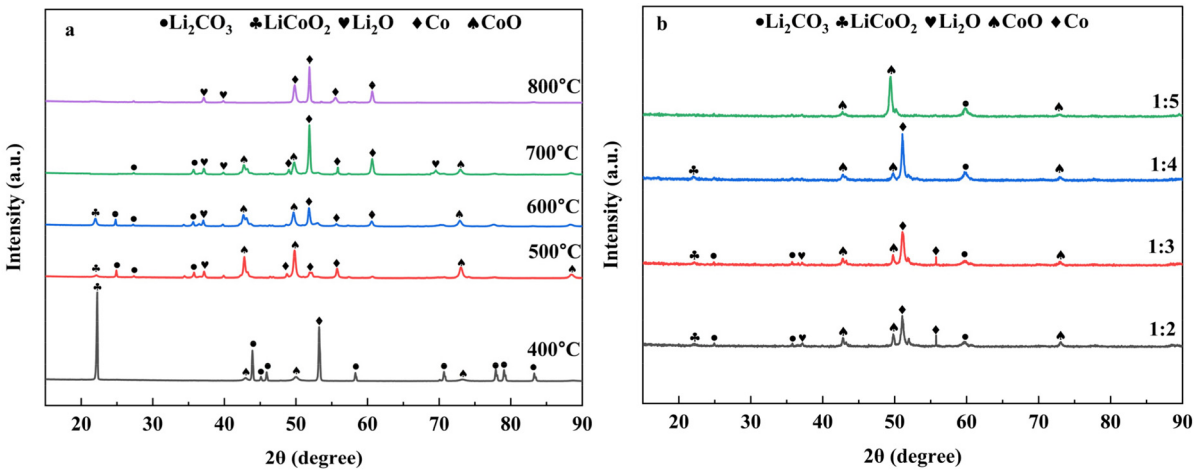

Fig. 4 XRD patterns of the products obtained from (a) the mixture of waste coffee powder and $LiCoO_2$ (mass ratio, 1 : 1) where coffee powder reduction thermal treatment was carried out at different temperatures for 90 min, (b) thermal treatment was carried out for 90 min at 600 °C temperature by varying the mass ratio of coffee powder and $LiCoO_2$.

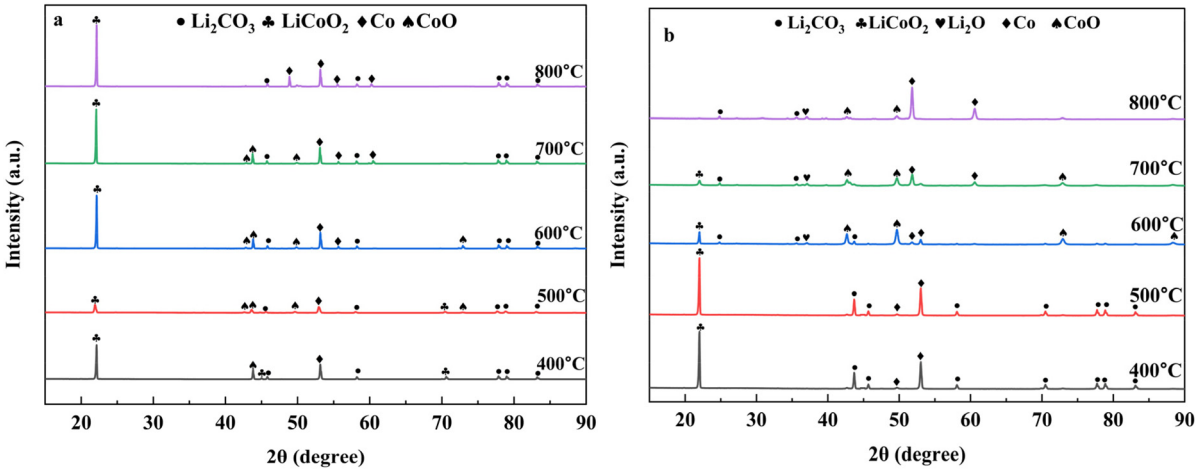

Fig. 5 XRD pattern of the product obtained from (a) pyrolysis gas reduction and (b) biochar reduction; in both cases the mass ratio was 1 : 1 and the operational time was 90 min.

coffee powder and $LiCoO_2$ were not mixed homogenously that is why only the gas generated from the coffee powder reacts with the $LiCoO_2$ which stimulates the starting of the reduction reaction. Another significant issue is that with the increasing of the reduction temperature, the presence of Li_2CO_3 does not change too much. From the biochar reduction thermal transformation (Fig. 5b) it is shown that $LiCoO_2$ is totally absent in the final products, this may be because of the effect of syngas and biochar which converted $LiCoO_2$ into more stable Li_2CO_3, Co, and CoO. The presence of Li_2O is also observed from the products obtained at 600 °C, 700 °C, and 800 °C temperature. Due to the reaction between the reducing agent and $LiCoO_2$, this Li_2O is generated. From temperatures 600 °C to 800 °C, the Li recovery efficiency in this process is almost similar to the coffee powder reduction which indicates that in the coffee powder reduction process, Li recovery at higher temperatures is regulated by the biochar reduction.

3.4 Percentage of lithium and cobalt recovery

After coffee powder reduction thermal transformation at a mass ratio of 1 : 1 at 600 °C temperature for 90 min, the product was subjected to water leaching. By evaporating the water from the leaching solution Li_2CO_3 was separated (Fig. 6a) and Co and CoO were obtained from the leachate precipitate (Fig. 6b). The elemental analysis of Li_2CO_3 and Co/CoO is presented in Table S1.†

Under different experimental conditions, the recovery efficiency of Li and Co was measured by analyzing the Li and Co concentration from the obtained filtered and precipitated products respectively which is presented in Fig. 7.

From Fig. 7a, it has been observed that with the increasing operational temperature from 400 °C to 600 °C the leaching efficiency of both the Li and Co was increased from 74.38% and 69.76% to 89.23% and 93.27%, respectively. This phenomenon was observed because, during the heating period, the reduction rate gradually increased. However, when the temperature was raised from 600 °C to 800 °C temperature, the recovery efficiency of both the Li and Co was decreased to 63.34% and 71.24% respectively. The reason behind this is that as the melting point of Li_2CO_3 is 722 °C they may be volatilized at higher temperatures. Another possible reason is that because of the utilization of too little amount of the laboratory dose, after reduction at higher temperatures, a small amount of product was obtained. The maximum recovery efficiency was observed at 600 °C for both Li and Co which is why this temperature was selected as an optimal temperature. The effect of the mass ratio of coffee powder and $LiCoO_2$ on the recovery of Li and Co is presented in Fig. 7b. With the decreasing mass ratio, the recovery efficiency of Li was slightly decreased to 72.93% while the recovery efficiency of Co was decreased significantly to 51.01%. The results indicate that the Li recovery efficiency is not affected significantly by the mass ratio of coffee powder and $LiCoO_2$, but the recovery efficiency of Co was to some extent affected by the amount of coffee powder. The effect of heating time on the recovery of Li and Co is shown in Fig. 7c. With the variation of the heating time, the recovery efficiency of both the Li and Co was varied. When the heating time shifted from 15 min to 90 min, the recovery efficiency of Li and Co also shifted from 48.51% and 33.23% to 89.23% and 93.98% respectively. The maximum efficiency was found when the heating time was 90 min, indicating that all the reactions were completed within 90 minutes.

Fig. 8a and b illustrate the Li and Co recovery efficiency from the products obtained from gas reduction and biochar reduction at different temperatures. During the gas reduction (Fig. 8a), the recovery efficiency of Li did not change significantly. This might be because as we observed from the XRD pattern of the gas reduction product (Fig. 5a), with the variation of the operational temperature $LiCoO_2$ was still present in the mixture because there were not enough gases that could react completely with it. On the other hand, with the increase of the temperature the amount of Co or CoO was increased

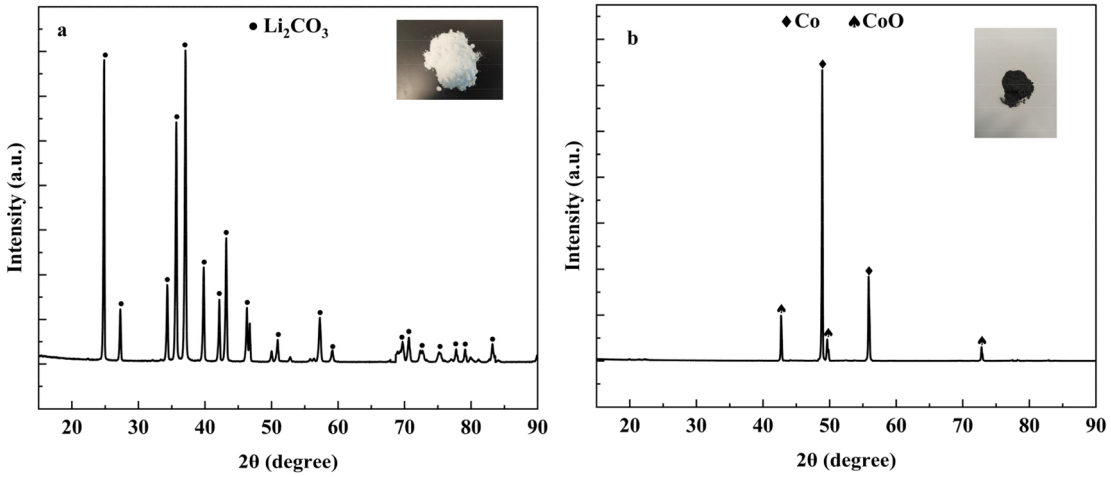

Fig. 6 XRD pattern of the product obtained from (a) evaporating the water from the leaching solution and (b) precipitation.

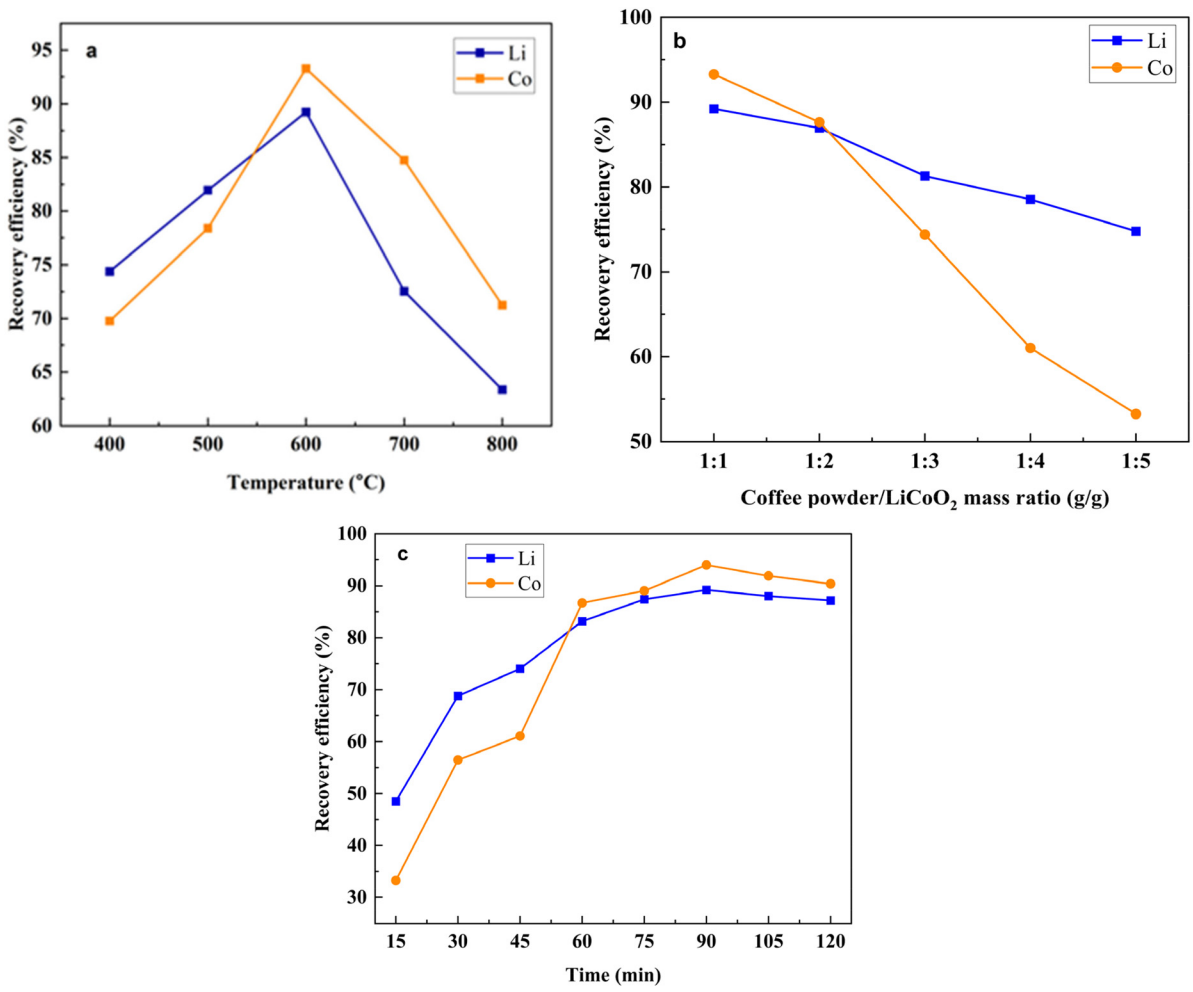

Fig. 7 Lithium and cobalt recovery efficiency in the coffee powder reduction process as a function of (a) temperature, (b) mass ratio, and (c) time.

(Fig. 5a), that's why the recovery efficiency of the Co was increased significantly (Fig. 8a). In gas reduction, the maximum recovery efficiency of Li and Co was obtained at 800 °C temperature and the amounts were 70.47% and 64.98% respectively. From Fig. 4b it has been observed that from the temperature 600 °C to 800 °C, both the Li and Co recovery

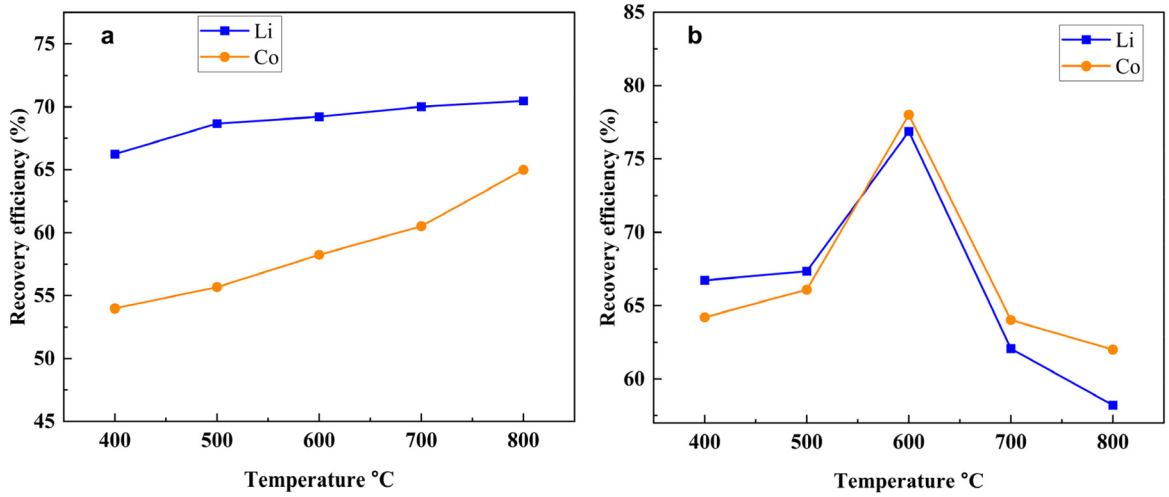

Fig. 8 Lithium and cobalt recovery efficiency (a) gas reduction (b) biochar reduction.

efficiencies of the biochar reduction process were almost similar to the coffee powder reduction (Fig. 4a) which indicates that in the coffee powder reduction process Li and Co recovery at higher temperature is regulated by the biochar reduction. However, the maximum recovery efficiency for both the Li and Co in the biochar reduction process was smaller than the coffee powder reduction process because the amount of gases generated from the biochar reduction was lower than the coffee powder reduction (Fig. S8†).

In conclusion, the coffee powder reduction showed maximum efficiency compared to the other two methods because in coffee powder reduction all the gases and carbon can react properly with the $LiCoO_2$. Therefore, under the optimized conditions when the temperature is 600 °C, the mass ratio of coffee powder and $LiCoO_2$ is 1 : 1 and the heating time is 90 min; the highest amount of Li (89.23%) and Co (93.27%) was recovered.

3.5 Conversion mechanism

There are two potential reasons for the conversion of CoO to Co_3O_4 during the calcination process. One is because of the inward diffusion of oxygen of CoO, the oxidizing reaction occurred and formed Co_3O_4 by following the chemical reaction:

$$3CoO + \frac{1}{2}O_2 \rightarrow Co_3O_4. \quad (12)$$

Another possible reason is that during the calcination process, Co_3O_4 is formed from CoO due to the decomposition of the preferred sites of CoO. The displacement reaction has occurred according to the following reaction:

$$4CoO \rightarrow Co_3O_4 + Co_i^{\bullet\bullet} + 2e' . \quad (13)$$

However, the oxidation mechanism is only responsible for the formation of Co_3O_4 along the outer boundaries of CoO, from which the inward diffusion of the oxygen takes place.[36] So, by following this mechanism, it is quite impossible to fully convert CoO to Co_3O_4. Therefore, it can be said that during the calcination of CoO, the displacement reaction occurred according to eqn (13) and CoO fully converted to Co_3O_4. The phase composition of the regenerated Co_3O_4 is presented in Fig. S9.†

The XRD diffraction peaks at 22.17°, 36.60°, 43.21°, 52.73°, 65.90°, and 70.47° confirm the presence of Co_3O_4 as the predominant phase in the recovered product. The diffraction peaks were well matched with the standard reference JCPDS No. 03-065-3103.

During the calcination of Li_2CO_3 and Co_3O_4 for a longer period, the following solid-state reaction occurs and generates $LiCoO_2$.[37]

$$3Li_2CO_3 + 2Co_3O_4 + \frac{1}{2}O_2 \rightarrow 6LiCoO_2 + 3CO_2 \quad (14)$$

3.6 Characterization of regenerated $LiCoO_2$

The XRD pattern of the regenerated $LiCoO_2$ is shown in Fig. 9(a). The diffraction peaks were observed at 22.03°, 43.74°, 44.82°, 45.73°, 53.10°, 58.14°, 70.54°, 77.83°, 78.95° and 83.14° which revealed that the peaks were harmonized with the standard $LiCoO_2$ diffraction card (JCPDS no. 00-016-0427), confirming that the main material of the regenerated product was $LiCoO_2$ crystals. The BET surface area of the regenerated $LiCoO_2$ is illustrated in Fig. 9(b). From the figure, it was observed that the surface area of the regenerated $LiCoO_2$ was 0.5296 $m^2\ g^{-1}$, indicating that the regenerated $LiCoO_2$ was suitable for the utilization of a cathode material.[38] Fig. 9c depicts the Raman spectra of the regenerated $LiCoO_2$ under 532 nm excitation. In the hexagonal $LiCoO_2$, factor-group analysis with the space group $R\bar{3}m$ structure indicates that two strong Raman active vibrational modes are present at 465 and 576 cm^{-1}. These bands are mainly attributed to the oxygen vibrations corresponding to the O–Co–O bending (E_g) and Co–O stretching (A_{1g}).[39,40] The E_g and A_{1g} modes are caused because of the vibration of oxygen atoms along the *a*–*b* plane

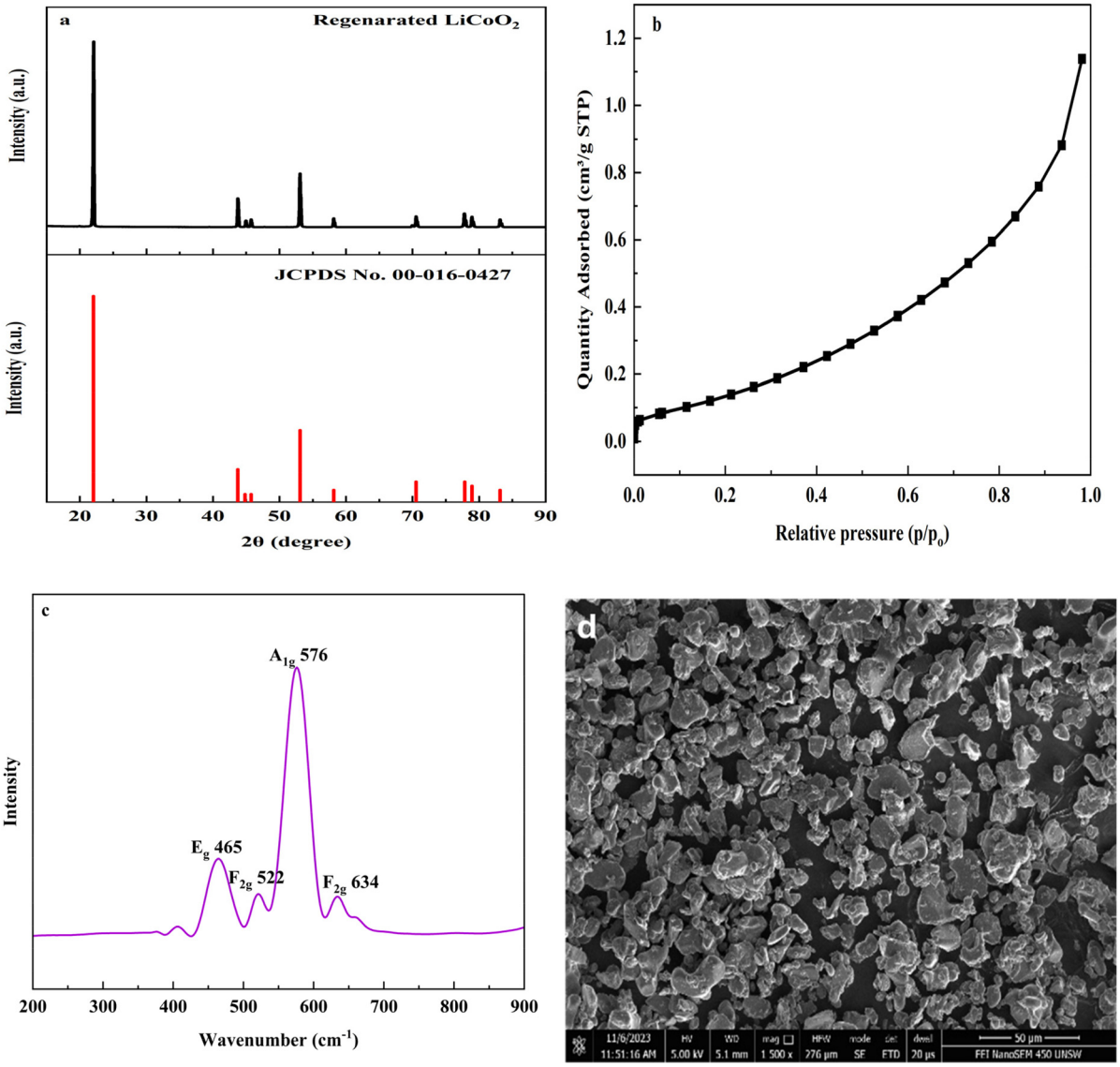

Fig. 9 Characterization of regenerated $LiCoO_2$: (a) XRD pattern; (b) BET surface area; (c) Raman spectra; (d) SEM.

and *c*-axis direction, respectively. Other two weak bands have been identified at 522 and 634 cm^{-1}, which correspond to the F_{2g} mode and the formation of these two bands indicates that Co_3O_4 is present in the samples.[41] Matsuda *et al.*[42] also observed similar types of bands during the charging and discharging of the Li_xCoO_2 cathode. The surface morphology of the regenerated $LiCoO_2$ was analyzed by SEM analysis and the SEM image of the regenerated $LiCoO_2$ is presented in Fig. 9d. From the figure, it can be seen that the regenerated $LiCoO_2$ was mostly spherical in shape with a smooth surface and non-homogeneous nature. The particle size of the regenerated $LiCoO_2$ was in the range of 2 μm to 8 μm. Many tiny particles may be attributed to the CO_3O_4 phase.

To identify the surface chemical state of the regenerated $LiCoO_2$ XPS analysis was carried out. Fig. S10(a–d)† show the XPS spectra collected at Li 1s, Co 2p, C 1s, and O 1s of the regenerated $LiCoO_2$. For all the sample peaks the calibration was conducted in terms of the C 1s species. The XPS spectra of Li 1s were observed at a binding energy of 54.23 eV (Fig. S7b†), confirming the presence of a metal oxide.[43] The XPS spectra of Co 2p are also observed in the regenerated $LiCoO_2$ which is further deconvoluted into four peaks. Three peaks were centered at 780.05 eV, 781.28 eV, and 782.84 eV for Co 2p3/2. Another peak was centered at 789.95 eV which is attributed to a satellite peak of Co-containing materials.[44] From the XPS spectra of the regenerated $LiCoO_2$ it was also observed that there are three deconvoluted peaks of C 1s (Fig. S7c†) at binding energies of 284.8 eV (C–C), 286.56 eV (C–O–C) and 289.84 eV (O–C=O).[45] From Fig. S10d† it has been observed that in the regenerated $LiCoO_2$, O 1s XPS spectra were deconvoluted into two peaks. One peak was centered at a binding energy of 529.71 eV, confirming the presence of a metal oxide,

and another peak was centered at a binding energy of 531.73 eV, justifying the presence of metal carbonates.

3.7 Electrochemical performance

Fig. 10a shows the charge–discharge curve of the regenerated $LiCoO_2$ in the 1st, 2nd, 5th, and 10th cycles between the voltages of 2.49 to 4.5 V at a rate of 1C (225 mA g^{-1}). The charge and discharge capacities of the regenerated $LiCoO_2$ electrode are 278.9 and 225.2 mA h g^{-1}, with an initial coulombic efficiency of 82.3%. This 1st cycle charge and discharge capacities are much higher than those of the commercial pristine $LiCoO_2$ (184.7 and 177.3 mA h g^{-1}) which was reported by Wang et al.[46] though they found higher coulombic efficiency (95.9%) than the present study. The regenerated $LiCoO_2$-containing electrode material shows low initial coulombic efficiency which may be because of the loss of active materials during the first charge–discharge cycle.[47] The initial discharge capacity of the regenerated $LiCoO_2$ electrode is lost at higher voltage which may be contributed by the Cathode–Electrolyte Interphase (CEI) formation because of the electrolyte

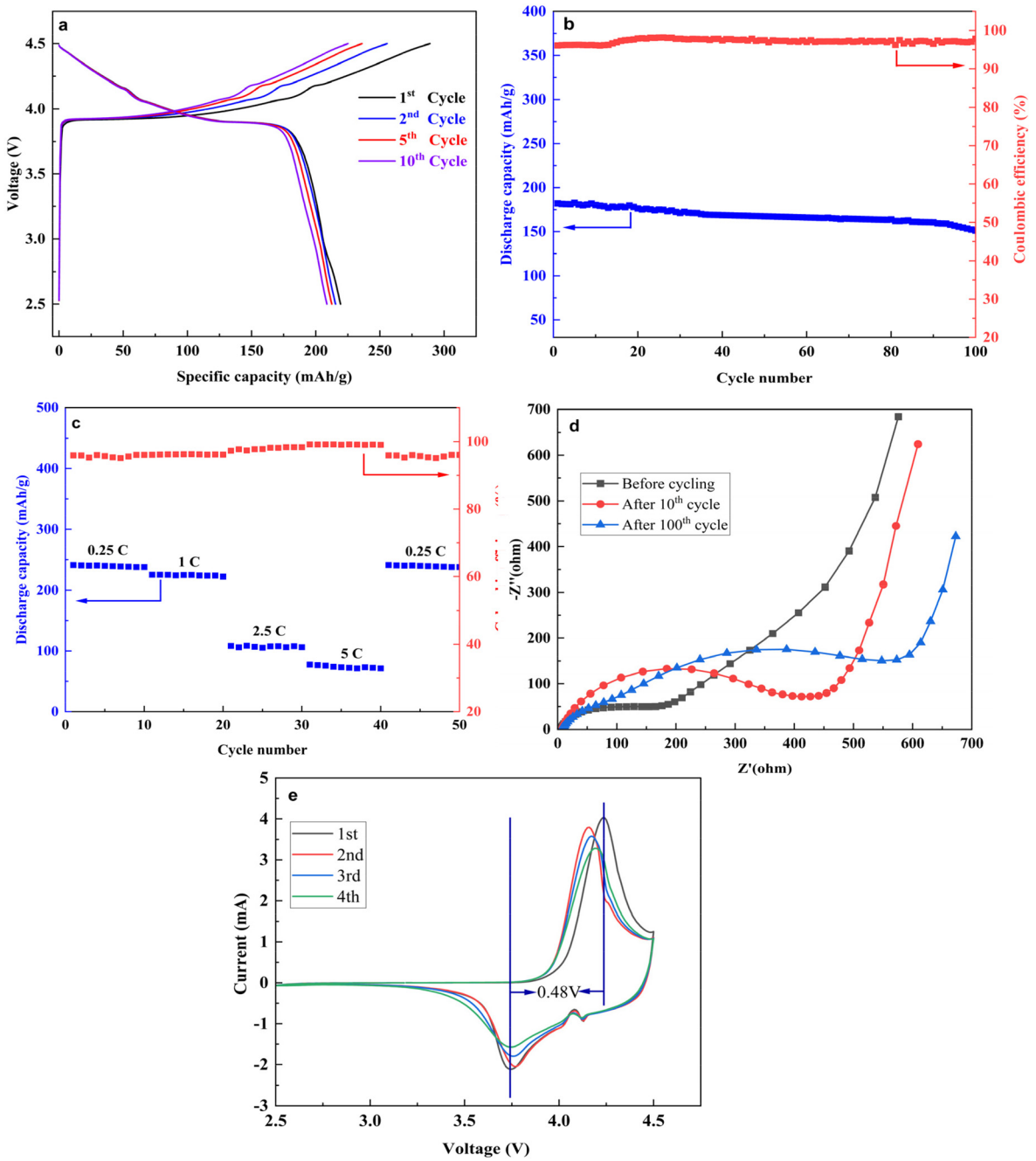

Fig. 10 (a) Charge–discharge curve; (b) cycle performance of the generated $LiCoO_2$; (c) rate performance; (d) EIS spectra; (e) CV curve of regenerated $LiCoO_2$.

decomposition.[48] From the graph in Fig. 10a it is also observed that in the voltage range of 4.15 to 4.49 V, the charge cut-off voltage of the $LiCoO_2$ coin cell does not show novel charge–discharge plateaus. Raising the cut-off voltage to 4.5 V indicates the delithiation values present in the range of 0.55 and 0.7 in $Li_{1-X}CoO_2$, in which the material structure mainly encircles the O_3 phase and the expansion capacity principally arising from solid solution reactions.[49] When using different cycles (1^{st}, 2^{nd}, 5^{th}, and 10^{th}) it can be found that the charging and discharging curves are almost stable. Moreover, at the 1^{st}, 2^{nd}, 5^{th}, and 10^{th} cycles, there is a slight difference between discharge and charge, indicating a little bit of polarization growth at the $LiCoO_2$ electrode. However, with the increase of the cycle, the Columbic efficiency gradually increased and at the 10^{th} cycle, the Columbic efficiency was 96% indicating superior charge–discharge reversibility. The electrode shows high specific capacity which may be because of the particle size of the regenerated $LiCoO_2$ which is close to 2 μm (Fig. 9d).

The cycling performance of the recovered $LiCoO_2$ is shown in Fig. 10b, at a rate of 1C in the voltage range of 2.5 to 4.5 V. The initial discharge capacity of the recovered $LiCoO_2$ electrode was 225.2 mA h g^{-1} and after 100 cycles the discharge capacity was retained to 189.1 mA h g^{-1} with the capacity retention rate of 83.2%. This result is better than that of most of the current studies on resynthesised or regenerated $LiCoO_2$. Xu *et al.*[49] observed that after 100 cycles the capacity retention rate of the pure $LiCoO_2$ electrode is 67.9%. In another study, Wang *et al.*[46] reported that the initial discharge capacity of the pristine $LiCoO_2$ electrode was 177.3 mA h g^{-1}, and after 100 cycles the discharge capacity was 145.5 mA h g^{-1} with a capacity retention rate of 82.1%. However, in the actual test, the discharge capacity is regulated by various factors. For example, due to the reaction of LiPF6 and the water present in the electrolyte HF was generated which further reacted with the active material and formed CEI film that demolished the active material and reduced the discharge capacity.[50] In conclusion, the recovered $LiCoO_2$ exhibits excellent cycling performance compared to other pure $LiCoO_2$, especially at a higher voltage of 4.5 V. Table 3 compares the cycling performances of the recovered $LiCoO_2$ and the previously reported $LiCoO_2$.

Fig. 10c illustrates the rate performance of the recovered $LiCoO_2$ in which the $LiCoO_2$ electrode was discharging at different rates (0.25C, 1C, 2.5C, and 5C). From the figure it has been observed that at a low rate of 0.25C, the recovered $LiCoO_2$ electrode shows the highest discharge capacity of 241.1 mA h g^{-1} which is uniform with the previous results. When the discharge current escalates, the discharge capacities of the $LiCoO_2$ electrode display varying degrees of depletion. At 1C, 2.5C, and 5C the discharge capacity of the $LiCoO_2$ electrode is 225.2, 108.4, and 77.6 mA h g^{-1} respectively. From the figure it is also seen that at 5C the discharge capacity of the $LiCoO_2$ electrode is 77.6 mA h g^{-1} which again increased to 241.1 mA h g^{-1} after returning to 0.25C, indicating the proper diffusion of lithium ions on the stable surface of $LiCoO_2$. Moreover, even at the highest rate of 5C, the recovered $LiCoO_2$ materials showed excellent performance with high coulombic efficiency which is close to 100%.

The electrochemical impedance spectra (EIS) of the recovered $LiCoO_2$ in three different stages: before cycling, after the 10^{th} cycle, and after the 100^{th} cycle are presented in Fig. 10d. The EIS spectra of the recovered $LiCoO_2$ cathode are composed of a semicircle in the high-frequency region which corresponds to the CEI film resistance (R_{CEI}) and another semicircle in the middle-frequency region that corresponds to the charge transfer resistance (R_{CT}). The oblique line in the low-frequency region because of the Warburg resistance indicates the lithium-ion diffusion ability of inactive material particles.[53] Moreover, the first intercept in the high-frequency region of the EIS spectra represents the lithium-ion impedance (R_f) on the surface layer of the electrode.[54] The calculated R_{CEI} values of the recovered $LiCoO_2$ electrode before cycling, after 10 cycles, and after 100 cycles were 6 Ω, 13 Ω, and 17 Ω, respectively. Before cycling, after 10 cycles, and after 100 cycles, the values of R_{CT} were 176.24 Ω, 441.11 Ω, and 593.10 Ω respectively. From the results, it has been observed that the R_{CEI} and R_{CT} values of the recovered $LiCoO_2$ cathode increased by 30.76% and 36.97% respectively, from the 10^{th} cycle to the 100^{th} cycle. After 100 cycles, the increment of the R_{CEI} and R_{CT} values of the $LiCoO_2$ electrode indicates that side reactions happen at the cathode–electrolyte interface and the growth of the CEI layer.[55]

Fig. 10e illustrates the first four CV curves of the regenerated $LiCoO_2$ in the range of 2.5–4.5 V. The predominant redox peaks (a1/c1) at around 4.2/3.7 V correspond to the Li^+ extraction/insertion process resulting from the redox reaction of Co^{3+}/Co^{4+}.[56] The minor redox peaks at around 4.1 V because of the phase transition between the two O_3 phases.[57] From the figure it has been also observed that between the two prominent redox peaks, there is a small voltage gap of 0.48 V and an overlap of the first four curves indicating the high reversibility of the electrochemical reaction and stability of the regenerated $LiCoO_2$. Besides, the

Table 3 Comparison of the electrochemical performance of the recovered $LiCoO_2$ and the previously reported $LiCoO_2$

Materials	Initial discharge capacity (mA h g^{-1})	Capacity retention ratio (%) (rate, cycle number)	Voltage window (V)	Ref.
Commercial $LiCoO_2$	206.1	82.8 (0.5C, 51)	3.0–4.55	51
Pristine $LiCoO_2$	177.3	82.1 (0.1C, 100)	2.5–4.5	46
Pristine $LiCoO_2$	202.9	67.32 (0.1C, 300)	3.0–4.5	52
MgF_2 coated $LiCoO_2$	180	80 (0.2C, 50)	3.0–4.5	50
Commercial $LiCoO_2$	162.9	73.11(0.2C, 100)	3.0–4.5	47
Recovered $LiCoO_2$	225.2	83.2 (1C, 100)	2.5–4.5	The present study

small peaks appeared around 4.1 V, coordinating the order–disorder transition which is depicted in Fig. 10a.

3.8 Analysis of environmental and economic aspects

By following the EverBatt model, the economic and environmental impacts of the direct recycling process (present study) were compared with the conventional hydrometallurgical and pyrometallurgical recycling technology. As hydrometallurgy technology is the most widely practiced method in the battery recycling industry the energy consumption, total cost, greenhouse gas emissions, and revenues are compared based on this technology. Assuming that a LIB recycling plant with an

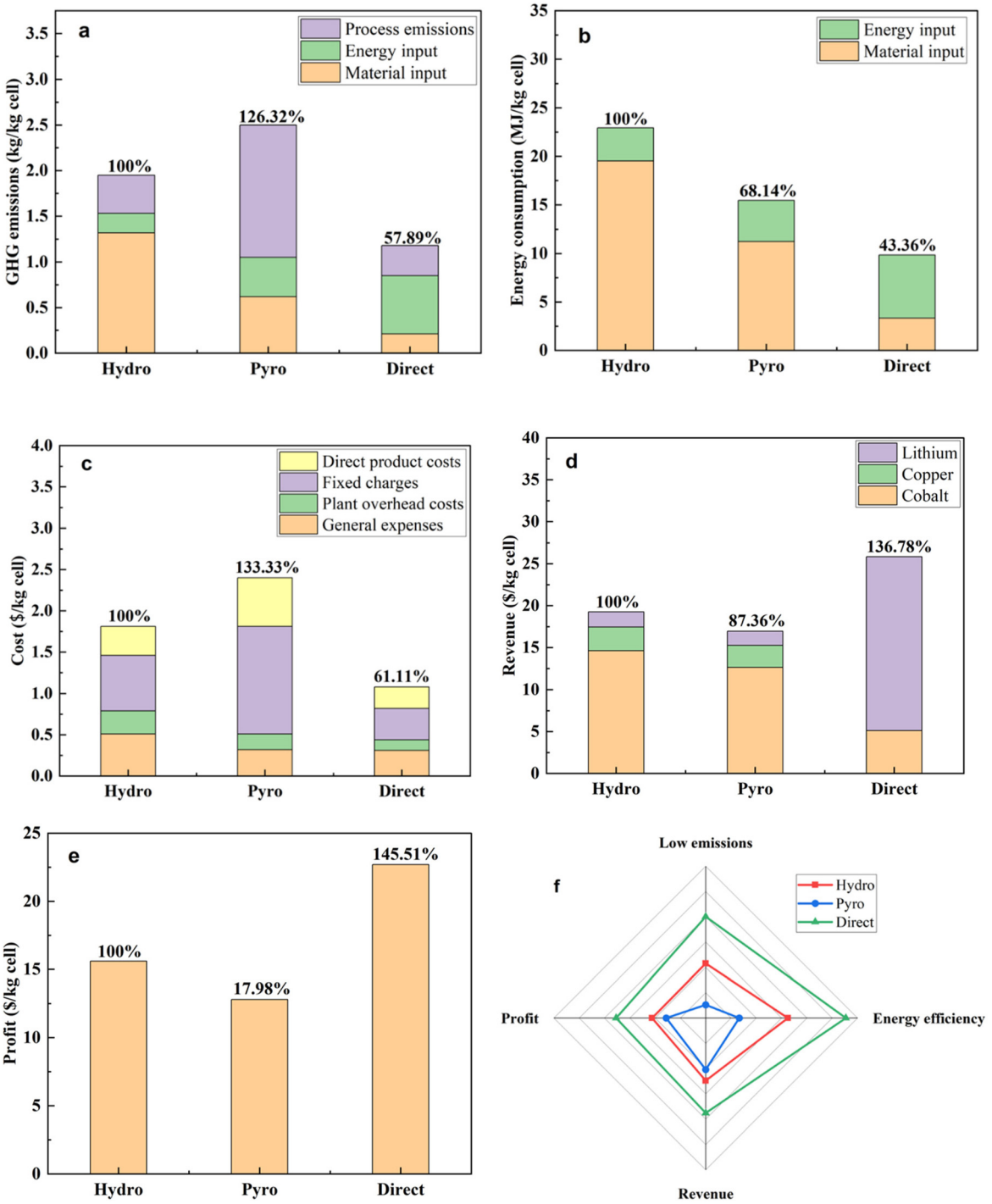

Fig. 11 Environmental and economic analysis of hydrometallurgy (Hydro), pyrometallurgy (Pyro), and direct recycling processes (present study): (a) greenhouse gas emissions (b) energy consumption (c) cost (d) revenue (e) profit and (f) comparison of the performances of hydro, pyro, and direct recycling processes.

annual capacity of 10 000 t applies three recycling technologies, the result with respect to greenhouse gas emissions, energy consumption, cost, and revenues of this plant is presented in Fig. 11(a–d). Greenhouse gas emission is one of the vital parameters to assess the environmental impact of recycling technologies. From Fig. 11(a) it has been observed that greenhouse gas emissions from the hydrometallurgy and pyrometallurgy recycling process are 1.93 and 2.41 kg kg^{-1} cathode cell respectively, whereas for direct recycling where coffee powder is used as an input material the greenhouse gas emissions are only 1.12 kg kg^{-1} cathode cell which is 57.89% of the hydrometallurgy. The high greenhouse gas emissions of these two conventional recovery technologies may come from the manufacturing process of a number of raw materials. Another important point is that in direct recycling the solutions of acid, alkali, and solvent were not used, whereas in the other two recycling techniques acids, alkalis, or solvents were used. From this discussion, it is quite clear that recycling coffee powder is more environmentally friendly than the other two commercial technologies. The energy consumption for the hydrometallurgy and pyrometallurgy recycling process is 22.62 and 15.41 MJ kg^{-1} cathode cell (Fig. 11b). On the other hand, for the coffee powder-assisted recycling process energy consumption is only 9.83 MJ kg^{-1} cathode cell which accounts for 43.36% of the hydrometallurgy recycling process. This high amount of energy is consumed in the two commonly used recycling technologies because of the high operational temperature and the characteristics of the input materials.

From the cost analysis in Fig. 11(c), it is observed that as the direct recycling process does not use a variety of input materials, or expensive equipment, this recycling technique is less expensive than the other two technologies. The cost beared in the direct recycling technique is \$1.13 per kg cathode cell which is only 61.11% of the hydrometallurgical technology.

Compared to two conventional recycling technologies (hydrometallurgy and pyrometallurgy), the coffee powder incorporated recycling technique shows the highest revenue (Fig. 11d). As the direct recycling technique shows the lowest cost and highest revenue which leads to the highest profit of \$23.62 from 1 kg of cathode material (Fig. 11e). One important point mentioned here is that the EverBatt model is a simple recycling method; the abovementioned economic analysis is not precise enough as the newly developed recycling technique has not been implemented on an industrial scale. However, in an open eye, we can observe at least three major advantages of the coffee powder incorporated recycling technique than the other two techniques. The major advantages are: (i) simple process and operational conditions, (ii) reduction of operational time and temperature, and (iii) elimination of the use of strong solvents, alkalis, and acids.

The spider chart illustrated in Fig. 11(f) shows a distinguishing difference among the recycling technologies. From the figure, it is clearly observed that in terms of low emissions, energy efficiency, revenue, and profit the coffee powder incorporated recycling technology is far better than the hydrometallurgy and pyrometallurgy process.

Conclusion

In summary, waste coffee powder has been recognized to be a potential reducing candidate to recover Li and Co from spent LIBs through a mild temperature pyrometallurgical process that is cost-effective and environmentally friendly. The maximum recovery efficiency of Li and Co was 89.23% and 93.27% respectively. Biomass reduced the temperature to 600 °C due to the generation of highly reactive gases such as H_2, CO_2, and CO which acted as reducing agents. To separate Li and Co from the pyrolyzed product, a water-leaching process was applied. This method is more environmentally friendly and economical because it eliminates the use of strong acids, bases, and solvents. Additionally, the regenerated $LiCoO_2$ showed excellent electrochemical performance with charge and discharge capacities of 278.9 and 225.2 mA h g^{-1} respectively. The cycling performance of the regenerated $LiCoO_2$ showed that after 100 cycles, 189.1 mA h g^{-1} discharge capacity was retained with a capacity retention rate of 83.2%. Even at the highest rate of 5C, the regenerated $LiCoO_2$ rate performance was 77.6 mA h g^{-1} with nearly 100% coulombic efficiency. This study provides a new method for regenerating $LiCoO_2$ from spent LIBs, which can be used as a cathode material in new LIBs. Overall, the proposed biomass-based reduction technique offers a cost-effective and eco-friendly approach to treating spent LIBs. The present study also makes a significant contribution to achieving several SDGs. We found that our study is closely related to the SDG 7, SDG 8, SDG 9, SDG 11, SDG 12, SDG 13, and SDG 15. In the future, different types of biomasses could be applied to recycle different types of LIBs containing various types of cathode materials, such as lithium nickel manganese cobalt oxide (LNMCO) and lithium manganese oxide (LMO).

Data availability

Data will be available on request.

Conflicts of interest

There are no conflicts to declare.

Acknowledgements

This research was supported by the Australian Research Council's Industrial Transformation Research Hub funding scheme (project IH190100009).

References

1 R. Kumar, C. Liu, G.-S. Ha, Y.-K. Park, M. Ali Khan, M. Jang, *et al.*, Downstream recovery of Li and value-added metals (Ni, Co, and Mn) from leach liquor of spent lithium-ion batteries using a membrane-integrated hybrid system, *Chem. Eng. J.*, 2022, **447**, 137507.
2 B. Swain, Recovery and recycling of lithium: A review, *Sep. Purif. Technol.*, 2017, **172**, 388–403.
3 Y. Ma, X. Zhou, J. Tang, X. Liu, H. Gan and J. Yang, One-step selective recovery and cyclic utilization of valuable metals from spent lithium-ion batteries via low-temperature chlorination pyrolysis, *Resour., Conserv. Recycl.*, 2021, **175**, 105840.
4 X. Zhang and M. Zhu, Recycling spent lithium-ion battery cathode: an overview, *Green Chem.*, 2024, **26**(13), 7656–7717.
5 L. Paoli and T. Gül, *Electric cars fend off supply challenges to more than double global sales*, 2022.
6 J. Wang, J. Ma, Z. Zhuang, Z. Liang, K. Jia, G. Ji, *et al.*, Toward Direct Regeneration of Spent Lithium-Ion Batteries: A Next-Generation Recycling Method, *Chem. Rev.*, 2024, **124**(5), 2839–2887.
7 E. Fan, L. Li, Z. Wang, J. Lin, Y. Huang, Y. Yao, *et al.*, Sustainable Recycling Technology for Li-Ion Batteries and Beyond: Challenges and Future Prospects, *Chem. Rev.*, 2020, **120**(14), 7020–7063.
8 S. Dang, W. Hou, Y. Min, J. Wu, Q. Xu and P. Shi, Electro-oxidation: A win–win strategy for the selective recovery of Li^+ from spent lithium-ion batteries and the preparation of highly active catalysts, *Chem. Eng. J.*, 2022, **435**, 135169.
9 Q. Peng, X. Zhu, J. Li, Q. Liao, Y. Lai, L. Zhang, *et al.*, A novel method for carbon removal and valuable metal recovery by incorporating steam into the reduction-roasting process of spent lithium-ion batteries, *Waste Manage.*, 2021, **134**, 100–109.
10 M. Wang, Q. Tan and J. Li, Unveiling the Role and Mechanism of Mechanochemical Activation on Lithium Cobalt Oxide Powders from Spent Lithium-Ion Batteries, *Environ. Sci. Technol.*, 2018, **52**(22), 13136–13143.
11 Y. Yang, E. G. Okonkwo, G. Huang, S. Xu, W. Sun and Y. He, On the sustainability of lithium ion battery industry – A review and perspective, *Energy Storage Mater.*, 2021, **36**, 186–212.
12 Y. Wang, N. An, L. Wen, L. Wang, X. Jiang, F. Hou, *et al.*, Recent progress on the recycling technology of Li-ion batteries, *J. Energy Chem.*, 2021, **55**, 391–419.
13 J. C.-Y. Jung, P.-C. Sui and J. Zhang, A review of recycling spent lithium-ion battery cathode materials using hydrometallurgical treatments, *J. Energy Storage*, 2021, **35**, 102217.
14 B. Makuza, D. Yu, Z. Huang, X. Guo, Q. Tian, K. Zhang, *et al.*, Synergetic carbothermic reduction and selective hydrochlorination of spent Li-ion batteries black mass towards enhanced metal recovery, *J. Cleaner Prod.*, 2023, **386**, 135831.
15 D. Dutta, R. Rautela, L. K. S. Gujjala, D. Kundu, P. Sharma, M. Tembhare, *et al.*, A review on recovery processes of metals from E-waste: A green perspective, *Sci. Total Environ.*, 2023, **859**, 160391.
16 K. K. Brar, S. Magdouli, S. Etteieb, M. Zolfaghari, H. Fathollahzadeh, L. Calugaru, *et al.*, Integrated bioleaching-electrometallurgy for copper recovery - A critical review, *J. Cleaner Prod.*, 2021, **291**, 125257.
17 P. Yadav, C. J. Jie, S. Tan and M. Srinivasan, Recycling of cathode from spent lithium iron phosphate batteries, *J. Hazard. Mater.*, 2020, **399**, 123068.
18 F. Su, X. Zhou, X. Liu, J. Yang, J. Tang, W. Yang, *et al.*, An efficient recovery process of valuable metals from spent lithium-ion batteries in acidic medium assisted with waste areca powder, *J. Environ. Chem. Eng.*, 2022, **10**(6), 108711.
19 D. Liu, Z. Su and L. Wang, Pyrometallurgically regenerated $LiMn_2O_4$ cathode scrap material and its electrochemical properties, *Ceram. Int.*, 2021, **47**(1), 42–47.
20 S. Park, S. Jung, D. Kwon, M. Beak, E. E. Kwon and K. Kwon, Carbothermic reduction of spent Lithium-Ion batteries using CO_2 as reaction medium, *Chem. Eng. J.*, 2022, **435**, 135165.
21 B. A. Nuraeni, K. Avarmaa, L. H. Prentice, W. J. Rankin and M. A. Rhamdhani, Carbothermic reduction of LiCoO2 cathode material: Thermodynamic analysis, microstructure and mechanisms, *Sustainable Mater. Technol.*, 2022, **34**, e00526.
22 Z. Yan, A. Sattar and Z. Li, Priority Lithium recovery from spent Li-ion batteries via carbothermal reduction with water leaching, *Resour., Conserv. Recycl.*, 2023, **192**, 106937.
23 J. Zhang, J. Hu, W. Zhang, Y. Chen and C. Wang, Efficient and economical recovery of lithium, cobalt, nickel, manganese from cathode scrap of spent lithium-ion batteries, *J. Cleaner Prod.*, 2018, **204**, 437–446.
24 F. Wang, D. Ouyang, Z. Zhou, S. J. Page, D. Liu and X. Zhao, Lignocellulosic biomass as sustainable feedstock and materials for power generation and energy storage, *J. Energy Chem.*, 2021, **57**, 247–280.
25 Y. Li, B. Xing, Y. Ding, X. Han and S. Wang, A critical review of the production and advanced utilization of biochar via selective pyrolysis of lignocellulosic biomass, *Bioresour. Technol.*, 2020, **312**, 123614.
26 Y. Zhao, B. Liu, L. Zhang and S. Guo, Microwave Pyrolysis of Macadamia Shells for Efficiently Recycling Lithium from Spent Lithium-ion Batteries, *J. Hazard. Mater.*, 2020, **396**, 122740.
27 F. Zhou, X. Qu, Y. Wu, J. Zhao, S. Gao, D. Wang, *et al.*, Vacuum Pyrolysis of Pine Sawdust to Recover Spent Lithium Ion Batteries: The Synergistic Effect of Carbothermic Reduction and Pyrolysis Gas Reduction, *ACS Sustainable Chem. Eng.*, 2022, **10**(3), 1287–1297.
28 F. Zhou, H. Wang, S. Wang, J. Zhao, X. Qu, D. Wang, *et al.*, Balancing the Components of Biomass and the Reactivity of Pyrolysis Gas: Biomass-Assisted Recycling of Spent $LiCoO_2$ Batteries, *Environ. Sci. Technol.*, 2024, **58**(4), 2102–2111.

29 S. Biswal, F. Pahlevani and V. Sahajwalla, Synthesis of Value-Added Ferrous Material from Electric Arc Furnace (EAF) Slag and Spent Coffee Grounds, *JOM*, 2021, **73**(6), 1878–1888.
30 R. Hossain and V. Sahajwalla, Molecular recycling: A key approach to tailor the waste recycling for high-value nano silicon carbide, *J. Cleaner Prod.*, 2021, **316**, 128344.
31 T. U. Han, J. Kim and K. Kim, Use of spent coffee ground as a reducing agent for enhanced reduction of chromate by freezing process, *J. Ind. Eng. Chem.*, 2021, **100**, 310–316.
32 W.-T. Tsai, S.-C. Liu and C.-H. Hsieh, Preparation and fuel properties of biochars from the pyrolysis of exhausted coffee residue, *J. Anal. Appl. Pyrolysis*, 2012, **93**, 63–67.
33 K. Johnson, Y. Liu and M. Lu, A Review of Recent Advances in Spent Coffee Grounds Upcycle Technologies and Practices, *Front. Chem. Eng.*, 2022, **4**, 838605.
34 H. W. Lee, A. Farooq, S.-H. Jang, E. E. Kwon, J. Jae, S. S. Lam, *et al.*, Enhanced bioaromatics synthesis via catalytic co-pyrolysis of cellulose and spent coffee ground over microporous HZSM-5 and HY, *Environ. Res.*, 2020, **184**, 109311.
35 Q. Dai, J. Spangenberger, S. Ahmed, L. Gaines, J. Kelly and M. Wang, *EverBatt: A Closed-loop Battery Recycling Cost and Environmental Impacts Model*, Argonne National Laboratory, 2019.
36 M. Żyła, G. Smoła, A. Knapik, J. Rysz, M. Sitarz and Z. Grzesik, The formation of the Co_3O_4 cobalt oxide within CoO substrate, *Corros. Sci.*, 2016, **112**, 536–541.
37 Y. Shi, G. Chen and Z. Chen, Effective regeneration of $LiCoO_2$ from spent lithium-ion batteries: a direct approach towards high-performance active particles, *Green Chem.*, 2018, **20**(4), 851–862.
38 P. Guan, L. Zhou, Z. Yu, Y. Sun, Y. Liu, F. Wu, *et al.*, Recent progress of surface coating on cathode materials for high-performance lithium-ion batteries, *J. Energy Chem.*, 2020, **43**, 220–235.
39 M. Inaba, Y. Iriyama, Z. Ogumi, Y. Todzuka and A. Tasaka, Raman study of layered rock–salt $LiCoO_2$ and its electrochemical lithium deintercalation, *J. Raman Spectrosc.*, 1997, **28**(8), 613–617.
40 T. Gross and C. Hess, Raman diagnostics of $LiCoO_2$ electrodes for lithium-ion batteries, *J. Power Sources*, 2014, **256**, 220–225.
41 V. Hadjiev, M. Iliev and I. Vergilov, The raman spectra of Co_3O_4, *J. Phys. C: Solid State Phys.*, 1988, **21**(7), L199.
42 Y. Matsuda, N. Kuwata, T. Okawa, A. Dorai, O. Kamishima and J. Kawamura, In situ Raman spectroscopy of $LixCoO_2$ cathode in $Li/Li_3PO_4/LiCoO_2$ all-solid-state thin-film lithium battery, *Solid State Ionics*, 2019, **335**, 7–14.
43 M. Wang, Q. Tan, Q. Huang, L. Liu, J. F. Chiang and J. Li, Converting spent lithium cobalt oxide battery cathode materials into high-value products via a mechanochemical extraction and thermal reduction route, *J. Hazard. Mater.*, 2021, **413**, 125222.
44 M. A. Ehsan, A. S. Hakeem and A. Rehman, Hierarchical Growth of CoO Nanoflower Thin Films Influencing the Electrocatalytic Oxygen Evolution Reaction, *Electrocatalysis*, 2020, **11**(3), 282–291.
45 Y. Zou, J. Cao, H. Li, W. Wu, Y. Liang and J. Zhang, Large-scale direct regeneration of $LiFePO_4$@C based on spray drying, *Ind. Chem. Mater.*, 2023, **1**(2), 254–261.
46 J. Wang, N. Wang, W. Nan, C. Wang, X. Chen, X. Qi, *et al.*, Enhancement of electrochemical performance of $LiCoO_2$ cathode material at high cut-off voltage (4.5 V) by partial surface coating with graphene nanosheets, *Int. J. Electrochem. Sci.*, 2020, **15**(9), 9282–9293.
47 Q. Tang, X. Dai, Z. Wang, F. Wu, Y. Mai, Y. Gu, *et al.*, Enhanced high-voltage performance of $LiCoO_2$ cathode by directly coating of the electrode with Li_2CO_3 via a wet chemical method, *Ceram. Int.*, 2021, **47**(14), 19374–19383.
48 G. Cherkashinin, K. Nikolowski, H. Ehrenberg, S. Jacke, L. Dimesso and W. Jaegermann, The stability of the SEI layer, surface composition and the oxidation state of transition metals at the electrolyte–cathode interface impacted by the electrochemical cycling: X-ray photoelectron spectroscopy investigation, *Phys. Chem. Chem. Phys.*, 2012, **14**(35), 12321–12331.
49 X. Xu, S. Zeng, B. Shen, W. Liu, M. Qin and W. Wang, Structural and electrochemical performance of F-doped SnO_2 coated $LiCoO_2$ as cathode materials, *Int. J. Electrochem. Sci.*, 2023, **18**(9), 100251.
50 H. J. Lee and Y. J. Park, Interface characterization of MgF_2-coated $LiCoO_2$ thin films, *Solid State Ionics*, 2013, **230**, 86–91.
51 P. Pang, Z. Wang, X. Tan, Y. Deng, J. Nan, Z. Xing, *et al.*, $LiCoO_2$@LiNi0.45Al0.05Mn0.5O_2 as high-voltage lithium-ion battery cathode materials with improved cycling performance and thermal stability, *Electrochim. Acta*, 2019, **327**, 135018.
52 F. Du, Z. Fan, L. Ding, Y. Wang, W. Shi, J. Zhang, *et al.*, Surface engineering based on element interdiffusion and interfacial reactions to boost the performance of $LiCoO_2$ cathode material, *Chem. Eng. J.*, 2023, **474**, 145952.
53 R. Tatara, P. Karayaylali, Y. Yu, Y. Zhang, L. Giordano, F. Maglia, *et al.*, The effect of electrode-electrolyte interface on the electrochemical impedance spectra for positive electrode in Li-ion battery, *J. Electrochem. Soc.*, 2019, **166**(3), A5090–A5098.
54 M. Umeda, K. Dokko, Y. Fujita, M. Mohamedi, I. Uchida and J. Selman, Electrochemical impedance study of Li-ion insertion into mesocarbon microbead single particle electrode: Part I. Graphitized carbon, *Electrochim. Acta*, 2001, **47**(6), 885–890.
55 Y. Sun, H. Dong, K. Wu, X. Chen, S. Wang, W. Gu, *et al.*, Graphene quantum dots coated $LiCoO_2$ for improved cycling stability and thermal safety at high voltage, *J. Electroanal. Chem.*, 2020, **866**, 114109.
56 L. Peng, Q. He, L. He, H. Lu, F. Zeng, B. Zheng, *et al.*, Improved electrochemical performance of a $LiCoO_2$/MCMB cell by regulating fluorinated electrolytes, *RSC Adv.*, 2021, **11**(49), 30763–30770.
57 J. Qian, L. Liu, J. Yang, S. Li, X. Wang, H. L. Zhuang, *et al.*, Electrochemical surface passivation of $LiCoO_2$ particles at ultrahigh voltage and its applications in lithium-based batteries, *Nat. Commun.*, 2018, **9**(1), 4918.